



# Insights on pH-dependent Physicochemical Properties and Supercapacitance Ability of $\alpha$ -MoO<sub>3</sub>

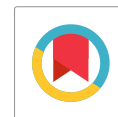
P. Janardhanan<sup>1</sup>, Varuna Jayachandran<sup>1</sup>, M. Elango<sup>1\*</sup> and J. Manikandan<sup>2</sup>

<sup>1</sup>Department of Physics, PSG College of Arts and Science, Coimbatore, TN, India

<sup>2</sup>Department of Chemistry, PSG College of Arts and Science, Coimbatore, TN, India

Received: 14.07.2024 Accepted: 09.09.2024 Published: 30.09.2024

\*elango@psgcas.ac.in



## ABSTRACT

The transition towards supercapacitors for efficient energy storage provides a dynamic outcome for the global warming. The MoO<sub>3</sub> samples were prepared at various pH using facile wet-chemical approach. The orthorhombic phase ( $\alpha$ -MoO<sub>3</sub>) was confirmed from structural investigations namely XRD, and Raman. It is also evident that the prepared samples show layered structure of MoO<sub>3</sub>, which contributed in improving the efficiency of the supercapacitor application. The morphological analysis from SEM micrographs showed a slight agglomeration. The CV studies revealed that the sample prepared at pH-10 displayed a higher specific capacitance.

**Keywords:**  $\alpha$  MoO<sub>3</sub>; Wet-chemical; Microstructure; Electrochemical properties; Electric double layer capacitor.

## 1. INTRODUCTION

A strong demand for a shift towards renewable and sustainable energy is the essential solution for addressing the alarming global warming and climate change. For electricity and transportation, the reliance on fossil fuel increases greenhouse gases production and intensifies the environmental challenges. Therefore, implementing renewable energy resources create promising sustainable future, where energy production and environmental preservation are in harmony by curbing greenhouse gas emissions (Mensah-Darkwa *et al.* 2019). Supercapacitors have significant part to replace batteries in hybrid electric vehicles and portable electronic devices with many interesting properties namely, high power output, prolonged operational lifespans, rapid cycling rates, remarkable stability, and durability. Supercapacitors made of inorganic materials show superior structural, electrical, storage properties along with a non-toxic nature, cost effective and eco-friendly (Thillaikkarasi and Ramesh, 2022). The various inorganic materials being researched like Fe<sub>2</sub>O<sub>3</sub>, CuO, NiO, and MnO<sub>2</sub> have gained a huge attention due to their lightweight architecture (Shao *et al.* 2021), (El-Nady *et al.* 2022; Yue *et al.* 2022). Among them, MoO<sub>3</sub> with unique structural properties unravel their potential role towards sensors, hydrogen storage, piezoelectric devices, electrocatalysts, batteries and supercapacitors. It is an n-type semiconductor with an energy gap of  $\geq 3$  eV (Kodan *et al.* 2018).

MoO<sub>3</sub> possesses three distinct polymorphs namely stable ( $\alpha$ -MoO<sub>3</sub>) orthorhombic, metastable ( $\beta$ -MoO<sub>3</sub>) monoclinic, and ( $h$ -MoO<sub>3</sub>) hexagonal. The phase of  $\alpha$ -MoO<sub>3</sub> consists of double-layered [MoO<sub>6</sub>] octahedral units. The  $\beta$ -MoO<sub>3</sub> displays a three-dimensional structure in which the corner oxygen atoms are shared by [MoO<sub>6</sub>] octahedra. The  $h$ -MoO<sub>3</sub> has a one-dimensional tunnel-like structure comprising a zigzag chain of [MoO<sub>6</sub>] octahedra. Among these phases,  $\alpha$ -MoO<sub>3</sub> is specifically well-suited for charge storage owing to its distinct layered structure parallel to the (010) direction, which provides open channels that enable the intercalation at various sites (Chithambararaj *et al.* 2016). The thermodynamically stable and 2D layered orthorhombic phase ( $\alpha$ ) of MoO<sub>3</sub> can be prepared by a simple precipitation approach with appreciable mechanical stability and specific capacitance. An appreciable specific capacitance value of around 240 F g<sup>-1</sup> was reported at a current density of 1.5 mA cm<sup>-2</sup> with a retention of 78.8% even after 5000 cycles was achieved by 2D  $\alpha$ -MoO<sub>3</sub> nanosheets synthesized via magnetron sputtering (Murugesan *et al.* 2019). Novel structure of MoO<sub>3</sub>/MoO<sub>3</sub>/SiO<sub>2</sub> prepared via electrodeposition shows the power density of about 1000 W Kg<sup>-1</sup> and with an energy density of 78 Wh Kg<sup>-1</sup> with around 98% cyclic stability over 8000 cycles, whereas, poly dispersed MoO<sub>3</sub> displayed a specific capacitance of 835 F g<sup>-1</sup> at 1 A g<sup>-1</sup>. In our current research,  $\alpha$ -MoO<sub>3</sub> were prepared through a simple wet chemical route and calcined at 500 °C (Zhao *et al.* 2020). The structural, morphological, optical, and capacitance properties of the samples were studied. The

electrochemical supercapacitance of the sample was tested for 1 M KOH as the electrolyte.

## 2. MATERIALS AND METHODS

### 2.1 Materials

The analytical grade precursor chemicals namely hexa ammonium hepta molybdate [(NH<sub>4</sub>)<sub>6</sub>Mo<sub>7</sub>O<sub>24</sub>·H<sub>2</sub>O], nitric acid [HNO<sub>3</sub>], liquid ammonia [NH<sub>3(l)</sub>] were purchased from Merck, India. All the chemicals are used without any further purification process.

### 2.2 Preparation Protocol

The MoO<sub>3</sub> samples at different pH were prepared by employing facile wet-chemical approach. Typically, 0.2 mol of molybdate precursor was dissolved in 100 ml of deionized water and left at constant stirring for 30 mins. After complete dissolution, 25 ml of concentrated Nitric acid (HNO<sub>3</sub>) was added in drops to the solution. The homogeneous mixture underwent a constant stirring at 85 °C for 3 hours, followed by the addition of precipitating agent [NH<sub>3</sub>] to the solution until pH-9 was attained. After that, formed precipitate was aged at room temperature for about 4 hours. The collected precipitate was centrifuged at 3000 rpm for 10 mins and rinsed thoroughly several times with acetone (CH<sub>3</sub>COCH<sub>3</sub>) and ethanol (CH<sub>3</sub>CH<sub>2</sub>OH) to remove the impurities. Then, the obtained precipitate after washing was dried at 120 °C for 24 hours. Later, the dried precipitate was calcined at 500 °C for 3 hours. Now, the MoO<sub>3</sub> sample prepared at pH-9 was collected and stored for characterization.

The aforementioned protocol was repeated for pH-10 and pH-11 as well. Finally, the samples prepared at different pH (9.0, 10.0, and 11.0) were analyzed for structural optical and super capacitance properties.

## 3. SAMPLE CHARACTERIZATION

The characterization techniques of structural and morphological investigations are XRD, Raman, and SEM. The three-electrode system was employed for recording the electrochemical activity of the samples with KOH as electrolyte.

## 4. RESULTS AND DISCUSSIONS

### 4.1 X-ray Diffraction

Fig. 1 presents the X-ray diffraction spectra of the as prepared samples and it form a basis for investigating the crystalline nature and phase purity of the samples. The MoO<sub>3</sub> samples prepared at different pH values exhibited orthorhombic crystal structure. The sharp and well-defined peaks indicate the multi-faceted

growth. The observed peaks at around ~12.8°, 23.1°, 25.7°, 27.2°, 29.6°, 33.8°, 35.5°, 38.9°, 46.1°, and 49.4° ascribes the miller planes (020), (110), (040), (021), (130), (111), (041), (060), (210), and (002) respectively. The absence of parasitic phase shows the phase purity of the samples prepared and the results accord well with the JCPDS card 05-0508 (space group - Pbnm (62)) (M. Shashank *et al.*, 2021). It is prominently evident that the planes (110), (040), and (021) at 23.1°, 25.7°, 27.2° respectively confirm stable orthorhombic (α-MoO<sub>3</sub>) phase that is thermodynamically stable. Thus, the unit cell parameters calculated was found to be a = 3.955 nm, b = 13.84 nm and c = 3.69 nm and are in relevant with the aforementioned JCPDS Card. The high-intense peaks imply the formation of layered structured of α-MoO<sub>3</sub> unit cells in anisotropic way (Usha *et al.* 2023). From the observed XRD spectra, d spacing, crystallite size, micro-strain, and other crystallographic parameters were found. The calculated microstructural attributes of the samples are tabulated in Table. 1 using the following relations.

$$n\lambda = 2d \sin\theta \quad (1)$$

$$D = (K \lambda) / (\beta \cos\theta) \quad (2)$$

$$\varepsilon = (\beta \cos \theta) / 4 \quad (3)$$

where, n is the order of reflection (n=1), d is the interplanar spacing (nm), θ be the Bragg's diffraction angle, D indicates crystallite size obtained from the Debye-Scherrer formula, β is the full width at half maxima, ε denotes micro-strain. The texture coefficient of (110) and (040) was lesser than (021) plane. The higher TC<sub>hkl</sub> of (021) attributes the better orientation due to insufficient interfacial energy, which eventually accelerates the nucleation and coalescence resulting in preferential orientation of the atoms in the specific direction (021) (Prakash *et al.* 2018).

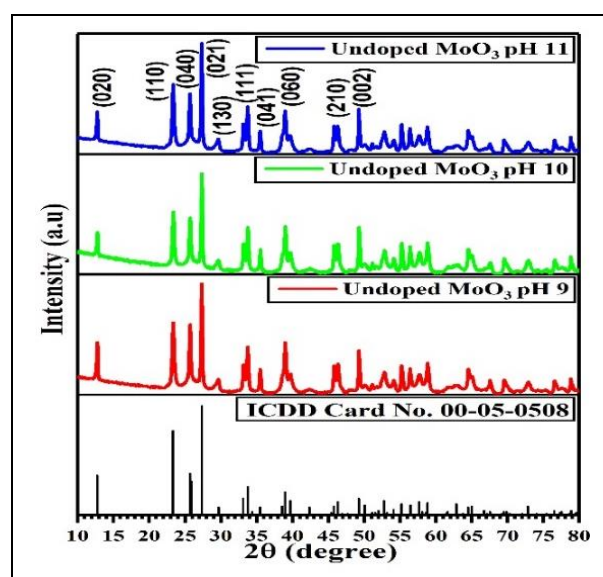


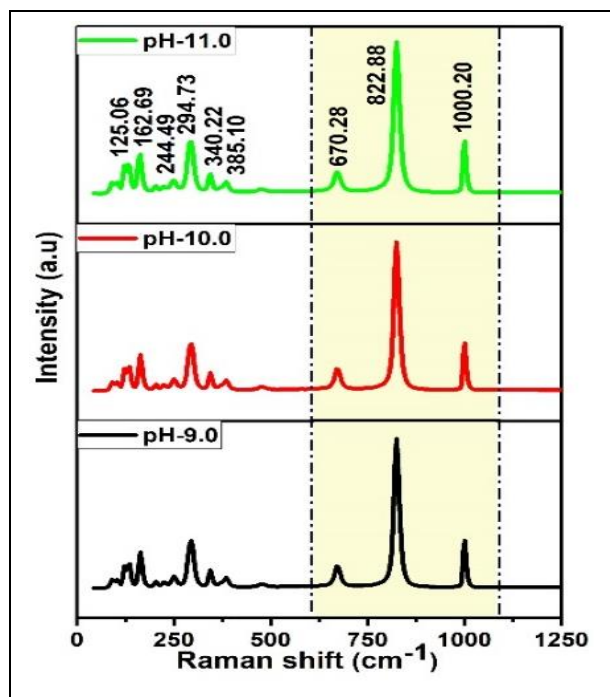
Fig. 1: XRD spectra of undoped MoO<sub>3</sub> nanoparticles at pH 9, pH 10 and pH 11

**Table. 1 Microstructural property of MoO<sub>3</sub> nanoparticles at pH 9, pH 10 and pH 11**

Samples	Crystallite size (nm)	Micro strain ( $\times 10^{-3}$ )
pH-9.0	48	0.0069
pH-10.0	45	0.0066
pH-11.0	46	0.0061

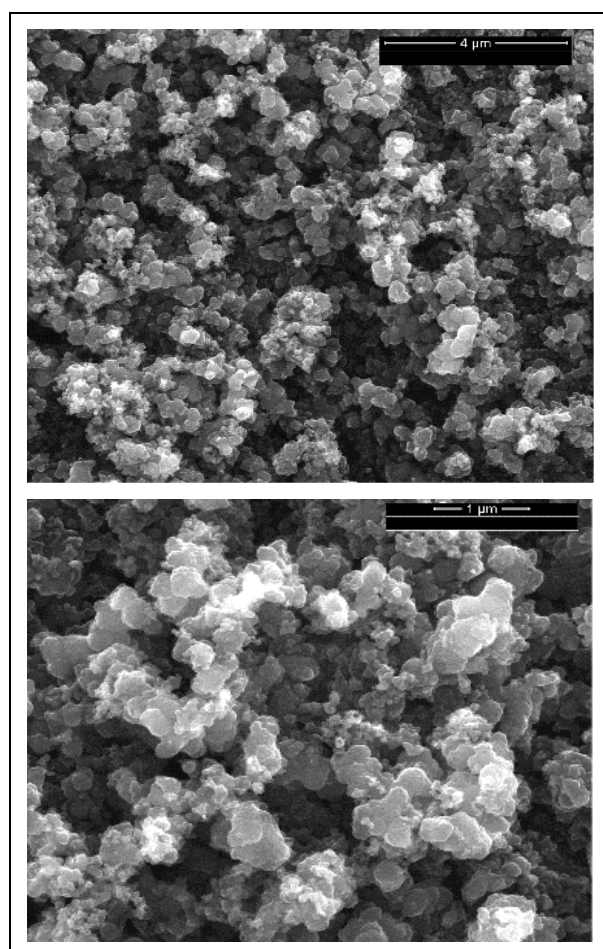
## 4.2 Raman Spectra

The vibrational spectra were recorded using a Raman laser excitation line to investigate the bonding nature and local structure of the prepared samples (Fig. 2). This effective tool provides information about the forces raised from mutual interactions of electrons and nuclei. The bands obtained from the spectra are assigned using Py - Masche model (Py and Maschke 1981). The characteristic Raman bands 670, 822, and 1000  $\text{cm}^{-1}$  attribute the layered configuration of orthorhombic MoO<sub>3</sub> structure. The 670  $\text{cm}^{-1}$  can be assigned to the symmetric stretching mode of triply coordinated bridge oxygen (Mo3-O: B2g, B3g) atoms and originated from sharing of oxygen located at the corner of the crystallites. The Raman bands around 822 and 1000  $\text{cm}^{-1}$  are symmetric (Mo<sup>2+</sup>O: Ag, B1g) and asymmetric (Mo<sup>6+</sup>=O: Ag, B1g) stretching modes of doubly coordinated oxygen and unshared oxygen atoms respectively (Shahsank *et al.* 2021) The bands at 340 and 385  $\text{cm}^{-1}$  can be related to the scissoring (B3g) and wagging (B1g) modes of O – Mo – O. The twisting and wagging modes of double bond O = Mo = O appeared around 244 (B3g) and 294 (B2g)  $\text{cm}^{-1}$  respectively. From the observed Raman spectra, it is evident that the prepared samples are orthorhombic in phase and it accords well with the XRD findings.

**Fig. 2: Raman Spectra of undoped MoO<sub>3</sub> nanoparticles at pH 9, pH 10 and pH 11**

## 4.3 SEM Analysis

The SEM micrographs of MoO<sub>3</sub> prepared at pH 10.0 is presented in Fig. 3. The SEM micrographs show non-uniform mere spherical morphology with sparse agglomeration. The particle's high surface energy stabilization might be the cause of the agglomeration. This was achieved via Ostwald's ripening process during growth of crystallites reaction (Lou and Zeng 2002). The particle size distribution calculated from the obtained micrograph exhibits ~ 20 nm. From the FESEM analysis, we realized that the individual particle boundaries in spite of particle agglomeration occur. Also, during the synthesis we have not exploited any form of surfactants in order to prevent the particle aggregation which results in mild agglomeration of particles.

**Fig. 3: SEM micrograph of undoped MoO<sub>3</sub> nanoparticles at pH 10**

## 4.4 CV Studies

The CV study of the prepared MoO<sub>3</sub> samples were recorded using a reference, working, auxiliary electrode workstation at various scan rates (10, 20, 30, 40, and 50 mV/s) in a potential window of -500 to 500 mV and are shown in Fig 4. The electrolyte of 1 M KOH was employed to study the electrochemical activity. The

CV graphs presented in Fig. 4, display the redox cycles of Faradaic reactions similar to electric double layer capacitor (EDLC). The specific capacitance of the MoO<sub>3</sub> synthesized at pH-9, 10, and 11 are 420, 460, and 333 F g<sup>-1</sup>. Among them, the pH<sup>-10</sup> prepared at a scan rate 10 mV/s exhibited the highest specific capacitance.

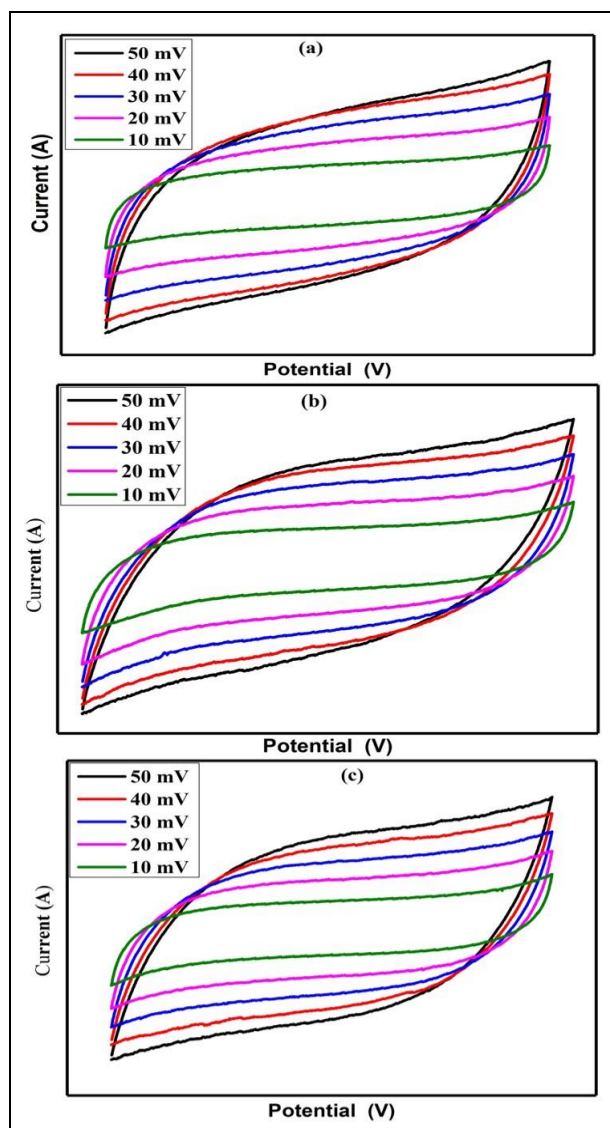


**Fig. 4:** Cyclic voltammetry analysis of undoped MoO<sub>3</sub> nanoparticles at pH 9 (a), pH 10(b) and pH 11(c)

## 5. CONCLUSION

The orthorhombic phase ( $\alpha$ ) MoO<sub>3</sub> were prepared at varying pH via simple co-precipitation method. The structural and morphological nature were analyzed through X-Ray diffraction, Confocal - RAMAN and Surface Emission Microscopy. The phase purity and multi-faceted growth were confirmed from the XRD and Raman. The layered structure of MoO<sub>3</sub> evidenced from the structural analysis are responsible for the witnessed electrochemical activity. The sparse agglomeration of non-uniform mere spherical morphology was revealed

from FESEM analysis. The pH-10 prepared MoO<sub>3</sub> exhibited the high specific capacitance.

## FUNDING

This research received no specific grant from any funding agency in the public, commercial, or not-for-profit sectors.

## CONFLICTS OF INTEREST

The authors declare that there is no conflict of interest.

## COPYRIGHT

This article is an open-access article distributed under the terms and conditions of the Creative Commons Attribution (CC BY) license (<http://creativecommons.org/licenses/by/4.0/>).



## REFERENCES

- Chithambararaj, A., Rajeswari Yogamalar, N. and Bose, A.C., Hydrothermally Synthesized h-MoO<sub>3</sub> and  $\alpha$ -MoO<sub>3</sub> Nanocrystals: New Findings on Crystal-Structure-Dependent Charge Transport, *Cryst Growth Des*, 16(4), 1984–1995 (2016). <https://doi.org/10.1021/acs.cgd.5b01571>
- Thillaikkarasi, D. and Ramesh, R., Synergetic Effect on Electrochemical Performance of Activated Carbon - Multiwalled Carbon Nanotubes Supercapacitor using various Electrodes in Aqueous Electrolyte, *J. Environ. Nanotechnol.*, 11(2), 04-21 (2022). <https://doi.org/10.13074/jent.2022.06.222453>
- El-Nady, J., Shokry, A., Khalil, M., Ebrahim, S., Elshaer, A. M. and Anas, M., One-step electrodeposition of a polypyrrole/NiO nanocomposite as a supercapacitor electrode. *Sci. Rep.*, 12(1), 3611 (2022). <https://doi.org/10.1038/s41598-022-07483-y>
- Kodan, N., Singh, A. P., Vandichel, M., Wickman, B. and Mehta, B. R., Favourable band edge alignment and increased visible light absorption in  $\beta$ -MoO<sub>3</sub>/ $\alpha$ -MoO<sub>3</sub> oxide heterojunction for enhanced photoelectrochemical performance, *Int. J. Hydrogen Energy*, 43(33), 15773–15783 (2018). <https://doi.org/10.1016/j.ijhydene.2018.06.138>
- Lou, X. W. and Zeng, H.C., Hydrothermal Synthesis of  $\alpha$ -MoO<sub>3</sub> Nanorods via Acidification of Ammonium Heptamolybdate Tetrahydrate, *Chem. Mater.*, 14 (11), 4781–4789 (2002). <https://doi.org/10.1021/cm0206237>

- Mensah-Darkwa, K., Zequine, C., Kahol, P. K. and Gupta, R. K., Supercapacitor Energy Storage Device Using Biowastes: A Sustainable Approach to Green Energy, *Sustainability*, 11(2), 414 (2019). <https://doi.org/10.3390/su11020414>
- Murugesan, D., Prakash, S., Ponpandian, N., Manisankar, P. and Viswanathan, C., Two dimensional  $\alpha$ -MoO<sub>3</sub> nanosheets decorated carbon cloth electrodes for high-performance supercapacitors, *Colloids Surf A Physicochem Eng. Asp.*, 569, 137–144 (2019). <https://doi.org/10.1016/j.colsurfa.2019.02.062>
- Prakash, N. G., Dhananjaya, M., Narayana, A. L., Shaik, D. P., Rosaiah, P. and Hussain, O.M., High Performance One Dimensional  $\alpha$ -MoO<sub>3</sub> Nanorods for Supercapacitor Applications, *Ceram. Int.*, 44 (8), 9967–9975 (2018). <https://doi.org/10.1016/j.ceramint.2018.03.032>
- Py, M. A. and Maschke, K., Intra- and interlayer contributions to the lattice vibrations in MoO<sub>3</sub>, *Physica B+C*, 105(1–3), 370–374 (1981). [https://doi.org/10.1016/0378-4363\(81\)90278-3](https://doi.org/10.1016/0378-4363(81)90278-3)
- Shahsank, M., Bhojya Naik, H. S., Sumedha, H. N. and Nagaraju, G., Implementing an in-situ carbon formation of MoO<sub>3</sub> nanoparticles for high performance lithium-ion battery, *Ceram Int*, 47 (7), 10261–10267 (2021). <https://doi.org/10.1016/j.ceramint.2020.07.241>
- Shao, W., Li, M., Wang, X., Fu, N. and Yang, Z., High-performance cobalt-doped carbon cloth supported porous Fe<sub>2</sub>O<sub>3</sub> flexible electrode material in quasi-solid asymmetric supercapacitors, *J. Alloys Compd*, 929, 167141 (2022). <https://doi.org/10.1016/j.jallcom.2022.167141>
- Usha, T., Ranjith Kumar, E., Kumar, M., Balraj, B., Sivakumar, C., Matheswaran, P., Chandrasekar, N. and Kumar Nagarajan, S., Physicochemical properties and photocatalytic activity of MoO<sub>3</sub> nanostructures: Evaluation of structural, optical, vibrational, and morphological properties, *Ceram Int*, 49(9), 13994–14006 (2023). <https://doi.org/10.1016/j.ceramint.2022.12.281>
- Yue, T., Shen, B. and Gao, P., Carbon material/MnO<sub>2</sub> as conductive skeleton for supercapacitor electrode material: A review. *Renew. Sustain. Energy Rev.* 158, 112131 (2022). <https://doi.org/10.1016/j.rser.2022.112131>
- Zhao, N., Fan, H., Zhang, M., Ma, J., Du, Z., Yan, B., Li, H. and Jiang, X., Simple electrodeposition of MoO<sub>3</sub> film on carbon cloth for high-performance aqueous symmetric supercapacitors, *Chem. Eng. J.*, 390, 124477 (2020). <https://doi.org/10.1016/j.cej.2020.124477>